Received: 30 December 2023 | Revised: 4 March 2024 | Accepted: 5 March 2024

DOI: 10.1002/nag.3725

SHORT COMMUNICATION

WILEY

Hydro-mechanically coupled CEL analyses with effective contact stresses

Patrick Staubach[1,2]

[1]Institute of Structural Engineering, Bauhaus-University Weimar, Weimar, Germany

[2]Foundation Engineering and Environmental Geotechnics, Ruhr-University Bochum, Bochum, Germany

Correspondence
Patrick Staubach, Chair of Geotechnics, Institute of Structural Engineering, Bauhaus-University Weimar, Germany.
Email: patrick.staubach@uni-weimar.de

Abstract

The coupled Eulerian–Lagrangian (CEL) method implemented in Abaqus is an established tool for modelling large deformations in numerical geomechanics. As shown in previous work, it can be extended to a hydro-mechanically coupled scheme by exploiting the similarity of the heat balance equation to the mass balance equation of fluids. However, the distinction between effective and total contact stresses has not been possible in this approach, which hinders its application to problems with interface friction as frictional stresses are calculated based on total normal contact stress. An approach to circumvent this problem is presented in this work. Its relevance is demonstrated by the simulation of vibratory pile driving model tests in water-saturated sand. The implementation by means of user-subroutines is available and works for any total-stress analysis.

KEYWORDS

coupled Eulerian–Lagrangian, friction, hydro-mechanically coupled, large deformations, pile driving

1 | INTRODUCTION

Modelling large deformations in geotechnical engineering is a very relevant yet challenging task. Many different schemes to tackle large deformation problems in continuum mechanics exists, of which the coupled Eulerian–Lagrangian (CEL) method is a promising tool.[1,7,17] Essentially, the CEL method allows to combine Eulerian and Lagrangian representation of continua within the same model considering interaction between the two region s.

The CEL method is becoming increasingly popular in solving large deformation problems in geomechanics, mainly because it is easily accessible, extendable and comparably user-friendly through the commercial programme package Abaqus.

In preceding works, the author presented the extension of the CEL method implemented in Abaqus to a hydro-mechanically coupled scheme, considering excess pore water pressures and consolidation (i.e. partially drained conditions),[12,13] which is based on the work presented in Refs. [2, 3] However, since total stresses are used in this approach in the balance of linear momentum of the mixture, and effective stresses are only distinguished in a user-defined material routine, total normal contact stresses are set into approach for the calculation of interface friction. Obviously, this results in wrong calculation of friction if the ratio of effective and total stresses changes during an analysis. Q1

This is an open access article under the terms of the Creative Commons Attribution-NonCommercial-NoDerivs License, which permits use and distribution in any medium, provided the original work is properly cited, the use is non-commercial and no modifications or adaptations are made.
© 2024 The Authors. *International Journal for Numerical and Analytical Methods in Geomechanics* published by John Wiley & Sons Ltd.

The aim of this work is to introduce a simple scheme which allows to calculate friction based on effective normal contact stresses instead of total stresses in CEL analyses. It is based on a modification of the coefficient of friction, which is formulated in dependence of the ratio of the effective to the total normal contact stresses.

The scheme presented in this work is not limited to CEL analyses but essentially resolves the aforementioned shortcomings in contact analyses for all total-stress analyses with Abaqus, including those utilising user-elements (see, e.g. Refs. [5, 6, 9]). To the author's best knowledge, no work-around solution for calculation of friction in CEL analyses has been presented yet as it poses additional difficulties compared to analyses with user-elements.

Note that all analyses presented in following are with reference to Abaqus 2023. It is recommended to use this release when adopting the procedures described in the following.

2 | HYDRO-MECHANICAL COUPLING USING A THERMO-MECHANICALLY COUPLED FORMULATION

In this section, it is briefly explained how the similarity between the set of differential equations used to account for hydro-mechanical coupling and the set of equations adopted for thermo-mechanical modelling can be exploited using Abaqus.[2,3] was the first to report on this approach for CEL analyses in the geotechnical community. However, in the original approach, the acceleration of the fluid (or solid) was not considered in the generalised Darcy-law, which is questionable for dynamic problems. In Refs., [12, 13] the approach by Refs. [2, 3] was subsequently supplemented by consideration of the missing acceleration term, building the basis of the present work. The approach is briefly recapped in this section.

A fluid saturated porous medium consisting of a solid phase $\sqcup^s$ and a fluid phase $\sqcup^w$ is considered. The balance of linear momentum of the mixture is given by [8]

$$\mathrm{div}(\boldsymbol{\sigma}) + \rho^{tot}\boldsymbol{b} = \rho^{tot}\ddot{\boldsymbol{u}}, \tag{1}$$

where $\boldsymbol{\sigma}$ is the total stress tensor, ρ^{tot} the total density of the mixture, $\boldsymbol{b}$ is the gravity vector and $\ddot{\boldsymbol{u}}$ is the acceleration of the solid phase (the acceleration of the fluid and the solid phase are assumed to be identical, see, for example, Refs. [10, 18] for a discussion on the influence of this assumption). The effective stress principle is applied to calculate the grain-to-grain stresses

$$\boldsymbol{\sigma}' = \boldsymbol{\sigma} + p^w\mathbf{I}, \tag{2}$$

wherein $\boldsymbol{\sigma}'$ corresponds to the effective stress tensor (compression negative), p^w is the pore fluid pressure (compression positive) and $\mathbf{I} = \mathrm{diag}[1, 1, 1]$ holds.

The balance of mass of the pore fluid is given by

$$\frac{n}{\bar{K}^w}\dot{p}^w + n\mathrm{div}(\dot{\boldsymbol{u}}^w) + (1-n)\,\mathrm{div}(\dot{\boldsymbol{u}}^s) = 0. \tag{3}$$

n is the porosity, $\bar{K}^w$ is the intrinsic bulk modulus of the fluid, $\dot{\boldsymbol{u}}^w$ and $\dot{\boldsymbol{u}}^s$ are the velocities of the pore fluid and the solid, respectively.

The balance of linear momentum of the pore fluid is used to calculate the relative velocity between the solid skeleton and the pore fluid, which is denoted as the generalised Darcy law given by

$$\boldsymbol{w}^w = \frac{\mathbf{K}^{\mathrm{Perm}}}{\eta^w}\cdot[-\mathrm{grad}(p^w) + \bar{\rho}^w(\boldsymbol{b} - \ddot{\boldsymbol{u}})], \tag{4}$$

with the density of the fluid $\bar{\rho}^w$, the permeability of the solid $\mathbf{K}^{\mathrm{Perm}} = \frac{k^w\eta^w}{\gamma^w}\mathbf{I}$, (with the hydraulic conductivity k^w and the specific weight of fluid γ^w) and the dynamic viscosity of the fluid η^w. Combining Equations (3) and (4), one obtains

$$\frac{n}{\bar{K}^w}\dot{p}^w - \frac{\mathbf{K}^{\mathrm{Perm}}}{\eta^w}\cdot\mathrm{div}[-\mathrm{grad}(p^w) + \bar{\rho}^w(\boldsymbol{b} - \ddot{\boldsymbol{u}})] - \mathrm{div}(\boldsymbol{v}^s) = 0. \tag{5}$$

UNCORRECTED PROOFS

Abaqus allows to couple the balance of linear momentum given by Equation (1) with the heat balance equation. The coupled thermal-stress equation solved for the temperature θ is given by

$$\rho c\dot{\theta} + k\ \mathrm{div}[\mathrm{grad}(\theta)] = -m_T, \tag{6}$$

for which the individual variables are of no importance as they will be replaced in the next step.

Equations (5) and (6) have the same general form of a convection–diffusion equation, whereby only the meaning of the material parameters is different. Combining Equations (5) and (6), one can find matching terms redefining the material parameters used in Equation (6), that is,

$$c \rightarrow \frac{n}{\bar{K}^w \rho^{tot}}, \tag{7}$$

$$k\ \mathrm{div}[\mathrm{grad}(\theta)] \rightarrow \frac{\boldsymbol{K}^{\mathrm{Perm}}}{\eta^w} \cdot \mathrm{div}[-\mathrm{grad}(p^w) + \bar{\rho}^w(\boldsymbol{b})] \quad \text{and} \tag{8}$$

$$m_T \rightarrow -\mathrm{div}(\dot{\boldsymbol{u}}^s) + \frac{\boldsymbol{K}^{\mathrm{Perm}}}{\eta^w}\mathrm{div}(\ddot{\boldsymbol{u}}). \tag{9}$$

With this redefinition, the temperature θ is equivalent to the excess pore fluid pressure, that is, $\theta = \Delta p^w$.

In the thermo-mechanically coupled analyses with Abaqus, Equations (1) and (6) are solved, but in Equation (6), the constants and m_T are replaced by the expressions given by Equations (7)–(9). Details on the implementation can be found in Refs. [12, 13] Spatially discretising Equation (1), the Neumann boundary condition being added contains a total stress traction vector. In order to fulfil equilibrium between interacting bodies, the contact stresses being added to this traction vector are expressed in terms of total stress as well. This leads to wrong calculation of frictional contact stresses, as is elaborated on in the next section.

3 | CALCULATION OF INTERFACE FRICTION

In order to derive a scheme for calculating frictional contact stresses based on effective normal contact stresses, the contact mechanic notation adopted in this work is introduced first.

According to Cauchy's stress theorem, the surface traction is defined by

$$\boldsymbol{t} = \boldsymbol{\sigma} \cdot \boldsymbol{n}, \tag{10}$$

wherein $\boldsymbol{n}$ is the normal vector of the surface and $\boldsymbol{t}$ is the total stress traction vector.

The contact stress of the contact pair can be separated in its normal and tangential components, namely,

$$\boldsymbol{t} = \boldsymbol{t}_N + \boldsymbol{t}_T. \tag{11}$$

The total normal stress component t_N (compression positive) is given by

$$t_N = \boldsymbol{n} \cdot \boldsymbol{\sigma} \cdot \boldsymbol{n}. \tag{12}$$

The total normal stress can be decomposed according to Terzaghi's principle in

$$t_N = t'_N + p^w, \tag{13}$$

where the effective normal contact stress t'_N is introduced. The tangential stress vector is defined by

$$\boldsymbol{t}_T = \boldsymbol{t} - \boldsymbol{t}_N = (\mathbf{I} - \boldsymbol{n} \otimes \boldsymbol{n}) \cdot \boldsymbol{t}. \tag{14}$$

The sliding condition ϕ represents the relationship between normal and tangential stress in the form of a constraint condition given by

$$\phi(\boldsymbol{t}_T, t'_N, \alpha) = ||\boldsymbol{t}_T|| - h(t'_N, \alpha) \leq 0, \tag{15}$$

UNCORRECTED PROOFS

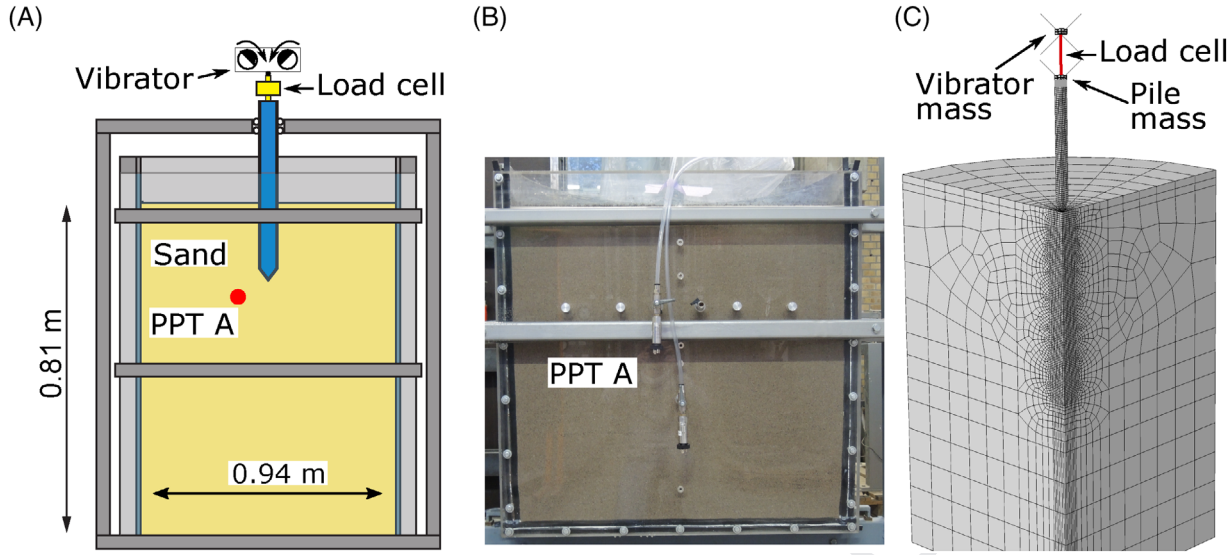

FIGURE 1 (A) Set-up of the model tests. (B) Photo of the test bench.[15] (C) CEL model.

where $h(t_N, \alpha)$ is a friction model describing the tangential resistance as a function of the effective normal stress t'_N and, potentially, the state variables α.

A simple relation for the sliding condition ϕ is obtained using the well-known Coulomb's law of friction given by

$$\phi = ||\boldsymbol{t}_T|| - \mu t'_N, \tag{16}$$

where μ is the friction coefficient. Two cases can be identified:

- The interacting bodies adhere to each other and the tangential contact stress $||\boldsymbol{t}_T||$ necessary for sliding is smaller than the resistance: $||\boldsymbol{t}_T|| < \mu t'_N$
- Sliding takes place: $||\boldsymbol{t}_T|| = \mu t'_N$

Following the procedures described in Section 2, the total normal stress t_N instead of the effective normal stress t'_N is set into approach when evaluating the friction model in the simulation using Abaqus. Therefore, a modified friction coefficient μ_{mod} would be required to obtain the same definition for ϕ, that is,

$$\phi = ||\boldsymbol{t}_T|| - \mu_{\text{mod}} t_N. \tag{17}$$

Unfortunately, it is not possible to modify the Coulomb friction model directly by means of a user-subroutine in case Eulerian elements are used in Abaqus[1]. However, it is possible to consider a (step-wise linear) dependency of the friction coefficient on so-called *field variables*. Field variables can be defined and updated using the information of the state variables of the constitutive model, which includes information about effective and total stresses. Therefore, a field variable may allow to express the ratio of the two stresses.

A modified friction coefficient μ_{mod} is introduced, which considers that total instead of effective normal contact stresses are used when evaluating Equation (17). Setting Equation (17) equal to Equation (16), one obtains the required modified friction coefficient as

$$\mu_{\text{mod}} = \mu \cdot \frac{t'_N}{t_N} = \mu \cdot \frac{t_N - p^w}{t_N}. \tag{18}$$

To realize the modified friction coefficient in the software, the term $\frac{t_N - p^w}{t_N}$ is defined as a field variable and the friction coefficient is made linearly depend on it, as it is the case according to Equation (18).

[1] This holds for all user-subroutines allowing for the modification of friction in explicit analyses using Abaqus 2023 or any earlier release, which are `VFRIC`, `VFRIC_COEF`, `VFRICTION`, `VUINTER`, and `VUINTERACTION`.

UNCORRECTED PROOF

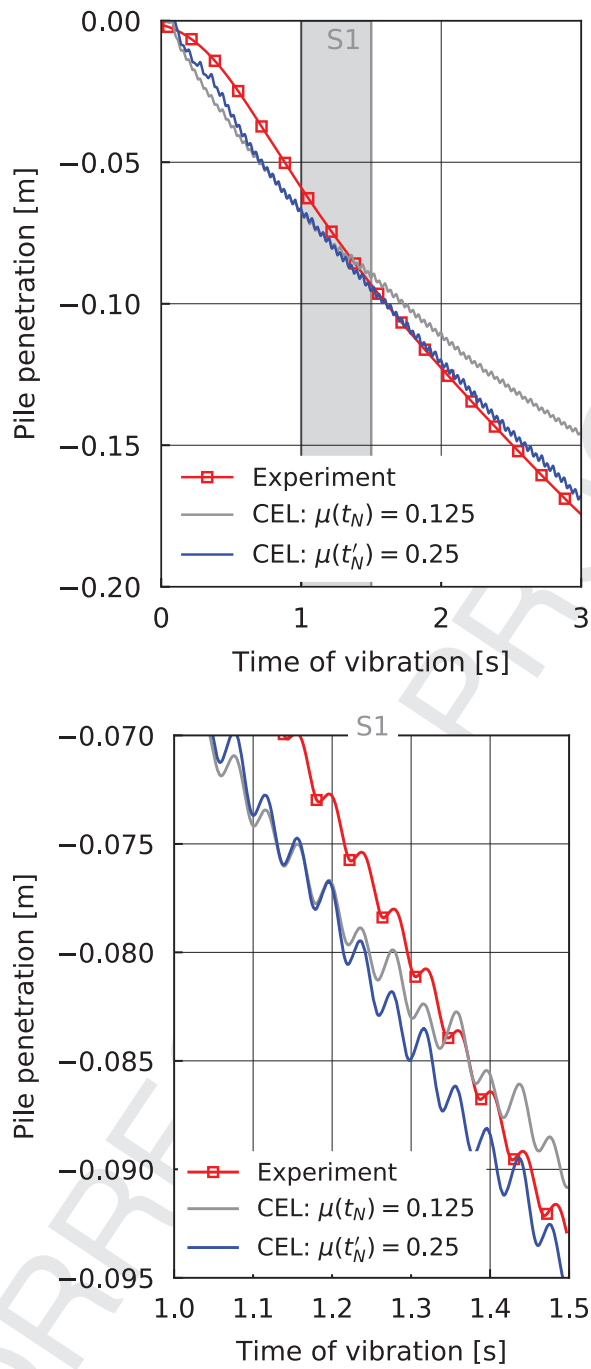

FIGURE 2 Pile penetration during vibratory pile driving for the values measured in the experiment (only the mean trend is depicted) and for the CEL simulation with correct calculation of friction ($\mu(t'_N) = 0.25$) or incorrect calculation of friction ($\mu(t_N) = 0.125$). The lower plot shows the grey section marked in the upper plot in detail.

Unfortunately, since the contact stress is oriented according to its local interface coordinate system, but all state variables of the constitutive model are given in a fixed global coordinate system at the integration points, a direct calculation of t_N or t'_N for a general 3D simulation is not possible (the CEL method is implemented only for 3D analyses in Abaqus). It is important to note that Abaqus distinguishes between field variables defined at the nodes and those defined at the integration points. Only field variables defined on the nodal level are considered if the friction coefficient is dependent on field variables. The procedures described above are all performed on the integration point level. Therefore, the field variables calculated in the integration points are mapped to the nodes, which is possible via the subroutines `VUFIELD` (field variables at the nodal level) and `VUSDFLD` (field variables at the integration point level). Since the normal vectors

UNCORRECTED PROOFS

for each node of the Lagrangian body can be calculated, an exact determination of the total and effective normal stress components is possible.

For example, pile driving being an axisymmetric problem, all normal vectors of the pile shaft pass through the centre of the pile axis. Therefore, all normal vectors of the soil elements are also defined to pass through the centre of the pile axis, so that they are orthogonal to the pile shaft for each point in space. Mathematically, a point on a circle with radius R and centre coordinates x_0, y_0 can be calculated using

$$R^2 = (x - x_0)^2 + (y - y_0)^2 \tag{19}$$

and its normal vector by

$$\boldsymbol{n} = \frac{[x - x_0, y - y_0]^T}{\sqrt{(x - x_0)^2 + (y - y_0)^2}}. \tag{20}$$

For the material points outside of the pile, Equation (20) has to be multiplied by −1, since the normal vector has to point to the pile shaft.

Note that for nonaxisymmetric boundary value problems this definition of the normal vectors must be revised. However, since the normal vectors can be defined as a function of the location of the nodes of the Lagrangian body, it is possible to consider complex surface geometries.

Following the calculation of the normal vector, the normal contact stress can be directly obtained based on the continuum stress components using Equation (12). The pore water pressure being a state variable of the constitutive model, it is known and needs not to be further modified.

It is important to note that Abaqus uses the average value of the field variable at the interface of two interacting bodies. If only one of the bodies has been assigned a value for a field variable, a value of zero will be automatically considered for the body not carrying values for the field variable (this holds for rigid and deformable bodies). Therefore, the ratio of effective to total stresses for which the regular friction coefficient μ is set into approach needs to be divided by two in this case.

4 | VIBRATORY PILE DRIVING MODEL TESTS IN WATER-SATURATED SAND

In Ref., [13] the simulation of model tests on vibratory pile driving in water-saturated 'Karlsruhe Sand' was performed using the approach introduced in Section 2, using total normal stresses to calculate friction. As is discussed in Ref., [13] this led to a worse accordance with the results of the model tests since the overestimation of interface friction resulted in too low pile penetration rates with increasing pile penetration. The simulation using the hydro-mechanically coupled CEL method is repeated in this work, adopting the scheme presented in the previous section, allowing for setting effective contact stresses in approach when calculating friction.

The model tests performed by *Vogelsang*[15,16] are briefly explained in the following. Figure 1A,B shows a schematic drawing and an image of the half-axisymmetric test device. A miniature vibrator was connected via a load cell with the pile. Pore pressure transducers (PPT A, see Figure 1) installed at the transparent front window were used to measure pore water pressures.

A closed-profile pile with a radius of 16.5 mm was used in the experiments. The aluminium pile had a smooth surface. The pile was pressed into the sand to a depth of around 15 cm before driving. While driving, the vibrator's 6.594-kg mass was entirely supported by the pile, allowing it to travel freely in a vertical direction. Likewise, only vertical movement of the pile was permitted by a guide. The combined mass of the pile, the load cell and the vibrator was 7.881 kg. The static moment of the vibrator was $5.33 \cdot 10^{-3}$ kg · m and the frequency of driving 25 Hz. To assure fully water-saturated conditions, the water table was held slightly above the ground level.

The experimental set-up is closely replicated in the numerical model depicted in Figure 1C. The masses of the individual components are considered and the load cell, with its corresponding spring stiffness, is modelled as well. The sinusoidal driving force is applied to the vibrator shown in Figure 1C. The hypoplastic model with intergranular strain extension is adopted as constitutive model. All specifications of the numerical model are the same as described in Ref. [13] For more detailed information, the interested reader is also referred to Ref. [11]

UNCORRECTED PROOFS

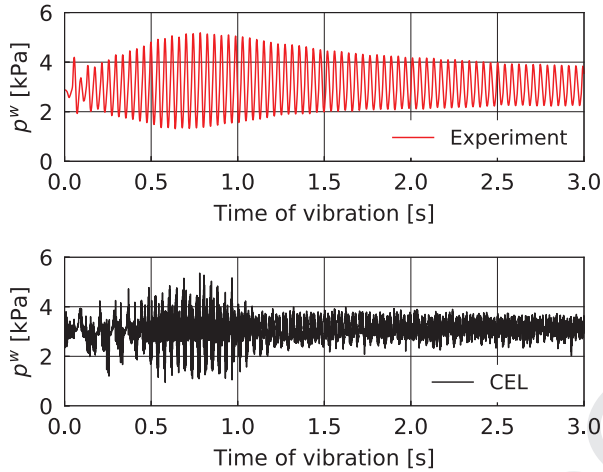

FIGURE 3 Pore water pressure p^w in PPT A measured in the experiment and predicted by the hydro-mechanically coupled CEL method with correct calculation of friction.

Friction between pile and soil is considered by a friction coefficient of $\mu = 0.25$. In addition to the analysis with correct calculation of friction (denoted as $\mu(t'_N) = 0.25$), a CEL simulation with a calculation of friction based on total normal stress t_N is considered (denoted as $\mu(t_N) = 0.125$). To account for the wrong calculation of frictional stresses in the simulation which considers total normal contact stresses, $\mu_{\text{mod}} = \mu/2 = 0.125$ is set into account. This is because the ratio of effective radial stresses to total radial stresses is identical to the ratio of the effective to the total dead weight initially, which is approximately 1/2 for the simulation. Clearly, this ratio changes during the simulation as the ratio of effective radial stresses to total radial stresses changes, for why friction is eventually not correctly calculated.

Before the vibratory driving starts in the simulations, the static load due to self-weight of the vibrator and pile is applied. This leads to a pile penetration of approximately 11 cm. The self-weight penetration is subtracted from the penetration shown in the following, such that only the penetration due to the vibratory pile driving process is evaluated.

The pile penetration versus time of driving plots are given for the values measured in the experiment and the results of the two simulations in Figure 2. The upper plot shows the complete time history and the lower plot gives the grey section in detail. At the beginning of the driving process, the simulation with correct calculation of friction predicts a lower penetration rate compared to the simulation using total normal contact stresses. This is because the effective contact stresses are much larger than the excess pore water pressures close to the ground surface as drainage is possible here. Therefore, friction is underestimated in case of $\mu(t'_N) = 0.25$.

As the penetration depth of the piles increases, this trend reverses between the simulations. This is because the shaft friction in the simulation with $\mu(t'_N) = 0.25$ is overestimated, as the excess pore water pressures reduce the effective contact stresses in reality. The simulation calculating friction correctly can consider this effect and gives results closer to the measured values.

The enlarged plot in the lower part of Figure 2 shows that the simulation with correct calculation of friction reproduces the experimental results more closely, both in terms of trend of penetration and amplitudes.

It is worth noting that the irregular movement of the pile with nonconstant amplitudes at the start of the driving (for the simulation $\mu(t'_N) = 0.25$) and in the grey section (for the simulation $\mu(t_N) = 0.125$) results from the uplift of the pile tip from the soil ('cavitational' driving), which has been investigated in detail in Ref. [14] This cannot be adequately considered in the simulation with the CEL method, as the separation of pile and water phase cannot be numerically prevented. Only with refined element formulations that discretise the fluid displacement or special hydro-mechanically coupled interface formulations is an adequate numerical representation possible.[14]

Finally, the pore water pressure p^w recorded in PPT A is compared for the measurements and the CEL simulation with correct calculation of friction in Figure 3. Note that in the CEL analysis, data are written with a high frequency (approximately every $3 \cdot 10^{-5}$ s) and no data smoothing is adopted. The comparison shows that the CEL simulation predicts both the amplitudes and the trend of the pore water pressure reasonably well. The pile passes the PPT A at approximately 0.8 s of driving, at which time both plots show the largest amplitudes of p^w. However, the CEL analysis shows

UNCORRECTED PROOFS

strong oscillations, for why the sinusoidal time history of the vibrator force is not well visible compared to the measured time history.

5 | CONCLUDING REMARKS

A simple approach to allow for the calculation of frictional contact stresses based on effective normal stresses in the framework of a hydro-mechanically coupled CEL formulation has been presented. The approach does not only resolve the problem of incorrect calculation of friction in CEL analyses, but in all other analyses working with total stresses in Abaqus (e.g. if locally undrained conditions are considered on the material model level or user-defined elements are used).

ACKNOWLEDGEMENTS

The author is grateful to Jakob Vogelsang for providing the experimental data.

DATA AVAILABILITY STATEMENT

All data, models or code that support the findings of this study are available from the corresponding author upon reasonable request. The implementation of the algorithms presented in this work (including the implementation of the hydro-mechanically coupled scheme and the hypoplastic model with intergranular strain extension) can be downloaded from the github repository https://github.com/patrickstaubach of the author.

ORCID

Patrick Staubach https://orcid.org/0000-0002-1788-4880

REFERENCES

1. Chen F, Liu L, Lai F, Gavin K, Flynn KN, Li Y. Numerical analyses of energy balance and installation mechanisms of large-diameter tapered monopiles by impact driving. *Ocean Eng*. 2022;266:113017. ISSN: 0029-8018.
2. Hamann T. *Zur Modellierung wassergesättigter Böden unter dynamischer Belastung und großen Bodenverformungen am Beispiel der Pfahleinbringung*. Institute of Geotechnical Engineering and Construction Management, University of Hamburg; 2015.
3. Hamann T, Qiu G, Grabe J. Application of a Coupled Eulerian-Lagrangian approach on pile installation problems under partially drained conditions. *Comput Geotech*. 2015;63:279-290. ISSN: 0266-352X.
4. Henke S. *Untersuchungen zur Pfropfenbildung infolge der Installation offener Pro252 file in granularen Böden. Habilitation*. Veröffentlichungen des Instituts für Geotech253 nik und Baubetrieb; 2014.
5. Liang J, Liang J. A user-defined element for dynamic analysis of saturated porous media in ABAQUS. *Comput Geotech*. 2020;126:103693. ISSN: 0266-352X.
6. Machaček J. *Contributions to the Numerical Modeling of Saturated and Unsaturated Soils*. Institut für Bodenmechanik und Felsmechanik am Karlsruher Institut für Technologie (KIT); 2020.
7. Qiu G, Henke S, Grabe J. Application of a coupled Eulerian-Lagrangian approach on geomechanical problems involving large deformation. *Comput Geotech*. 2011;38:30-39.
8. Schrefler BA, Scotta R. A fully coupled dynamic model for two-phase fluid flow in deformable porous media. *Comput Methods Appl Mech Eng*. 2001;190:3223-3246. Advances in Computational Methods for Fluid-Structure Interaction ISSN: 00457825.
9. Schümann B. *Beitrag zum dynamischen Dreiphasenmodell für Boden auf Basis der Finite-Elemente-Methode*. Veröffentlichungen des Instituts für Geotechnik und Baubetrieb der Technischen Universität Hamburg; 2015.
10. Staubach P, Machaček J. Influence of relative acceleration in saturated sand: analytical approach and simulation of vibratory pile driving tests. *Comput Geotech*. 2019;112:173-184. ISSN: 0266352X.
11. Staubach P. *Contributions to the Numerical Modelling of Pile Installation Processes and High-cyclic Loading of Soils*. Foundation Engineering and Environmental Geotechnics, Ruhr-University Bochum; Issue No. 73, 2022.
12. Staubach P, Machaček J, Moscoso MC, Wichtmann T. Impact of the installation on the long-term cyclic behaviour of piles in sand: a numerical study. *Soil Dyn Earthq Eng*. 2020;138:106223. ISSN: 02677261.
13. Staubach P, Machaček J, Skowronek J, Wichtmann T. Vibratory pile driving in water-saturated sand: back-analysis of model tests using a hydro-mechanically coupled CEL method. *Soils Found*. 2021;61:144-159. ISSN: 00380806.
14. Staubach P, Machaček J. Separating fluid and solid contact constraints for hydro-mechanically coupled finite elements discretising fluid displacement. *Comput Methods Appl Mech Eng*. 2023;416:116451. ISSN: 00457825.
15. Vogelsang J. *Untersuchungen zu den Mechanismen der Pfahlrammung*. Veröffentlichung des Instituts für Bodenmechanik und Felsmechanik am Karlsruher Institut für Technologie (KIT); 2016.
16. Vogelsang J, Huber G, Triantafyllidis T. Experimental Investigation of Vibratory Pile Driving in Saturated Sand. In: Triantafyllidis T, ed. *Holistic Simulation of Geotechnical Installation Processes*. Springer International Publishing; 2017:101-123. ISBN: 978-3-319-52590-7.

UNCORRECTED PROOFS

17. Wang D, Bienen B, Nazem M, et al. Large deformation finite element analyses in geotechnical engineering. *Comput Geotech*. 2015;65:104-114.
18. Zienkiewicz OC, Chang CT, Bettess P. Drained, undrained, consolidating and dynamic behaviour assumptions in soils. *Geotechnique*. 1980;30:385-395.

How to cite this article: Staubach P. Hydro-mechanically coupled CEL analyses with effective contact stresses. *Int J Numer Anal Methods*. 2024;1-9. https://doi.org/10.1002/nag.3725

UNCORRECTED PROOFS